On-Chip Surface-Enhanced Raman Spectroscopy using Nanosphere-Lithography Patterned Antennas on Silicon Nitride Waveguides

PIETER C. WUYTENS,[1,2,3,*] ANDRE G. SKIRTACH,[2,3] AND ROEL BAETS [1,3]

[1] *Photonics Research Group, INTEC Department, Ghent University-imec, Ghent, Belgium*
[2] *Department of Molecular Biotechnology, Ghent University, Ghent, Belgium*
[3] *Center for Nano- and Biophotonics, Ghent University, Belgium*
[*] *pieter.wuytens@ugent.be*

Abstract: A hybrid integration of nanoplasmonic antennas with silicon nitride waveguides enables miniaturized chips for surface-enhanced Raman spectroscopy at visible and near-infrared wavelengths. This integration can result in high-throughput SERS assays on low sampling volumes. However, current fabrication methods are complex and rely on electron-beam lithography, thereby obstructing the full use of an integrated photonics platform. Here, we demonstrate the electron-beam-free fabrication of gold nanotriangles on deep-UV patterned silicon nitride waveguides using nanosphere lithography. The localized surface-plasmon resonance of these nanotriangles is optimized for Raman excitation at 785 nm, resulting in a SERS substrate enhancement factor of 2.5×10^5. Furthermore, the SERS signal excited and collected through the waveguide is as strong as the free-space excited and collected signal through a high NA objective.

OCIS codes: (130.0130) Integrated optics; (130.6010) Sensors; (240.6695) Surface-enhanced Raman scattering; (220.4241) Nanostructure fabrication.

References and links

1. K. De Vos, I. Bartolozzi, E. Schacht, P. Bienstman, and R. Baets, "Silicon-on-Insulator microring resonator for sensitive and label-free biosensing," Optics Express **15**, 7610–7615 (2007).
2. E. Ryckeboer, R. Bockstaele, M. Vanslembrouck, and R. Baets, "Glucose sensing by waveguide-based absorption spectroscopy on a silicon chip." Biomedical Optics Express **5**, 1636–48 (2014).
3. A. Z. Subramanian, P. Neutens, A. Dhakal, R. Jansen, T. Claes, X. Rottenberg, F. Peyskens, S. Selvaraja, P. Helin, B. Dubois, K. Leyssens, S. Severi, P. Deshpande, R. Baets, and P. Van Dorpe, "Low-Loss Singlemode PECVD silicon nitride photonic wire waveguides for 532-900 nm wavelength window fabricated within a CMOS pilot line," IEEE Photonics Journal **5**, 2202809 (2013).
4. D. Martens, A. Z. Subramanian, S. Pathak, M. Vanslembrouck, P. Bienstman, W. Bogaerts, and R. G. Baets, "Compact silicon nitride arrayed waveguide gratings for very near-infrared wavelengths," IEEE Photonics Technology Letters **27**, 137–140 (2015).
5. X. Nie, E. Ryckeboer, G. Roelkens, and R. Baets, "Novel Concept for a Broadband Co-propagative Stationary Fourier Transform Spectrometer Integrated on a SiN Waveguide Platform," CLEO 2016 pp. 4–5 (2016).
6. E. P. Haglund, S. Kumari, P. Westbergh, J. S. Gustavsson, R. G. Baets, G. Roelkens, and A. Larsson, "20-Gb/s Modulation of Silicon-Integrated Short-Wavelength Hybrid-Cavity VCSELs," IEEE Photonics Technology Letters **28**, 856–859 (2016).
7. A. Z. Subramanian, E. Ryckeboer, A. Dhakal, F. Peyskens, A. Malik, B. Kuyken, H. Zhao, S. Pathak, A. Ruocco, A. D. Groote, P. Wuytens, D. Martens, F. Leo, W. Xie, U. D. Dave, M. Muneeb, P. V. Dorpe, J. V. Campenhout, W. Bogaerts, P. Bienstman, N. L. Thomas, D. V. Thourhout, Z. Hens, G. Roelkens, and R. Baets, "Silicon and silicon nitride photonic circuits for spectroscopic sensing on-a-chip," Photonics Research **3**, 47–59 (2015).
8. M. Mahmud-Ul-Hasan, P. Neutens, R. Vos, L. Lagae, and P. Van Dorpe, "Suppression of Bulk Fluorescence Noise by Combining Waveguide-Based Near-Field Excitation and Collection," ACS Photonics **4**, 495–500 (2017).
9. A. Dhakal, A. Z. Subramanian, P. C. Wuytens, F. Peyskens, N. Le Thomas, and R. Baets, "Evanescent excitation and collection of spontaneous Raman spectra using silicon nitride nanophotonic waveguides," Optics Letters **39**, 4025–4028 (2014).
10. A. Dhakal, P. Wuytens, A. Raza, N. Le Thomas, and R. Baets, "Silicon Nitride Background in Nanophotonic Waveguide Enhanced Raman Spectroscopy," Materials **10**, 140 (2017).

11. Z. Wang, M. N. Zervas, P. N. Bartlett, and J. S. Wilkinson, "Surface and waveguide collection of Raman emission in waveguide-enhanced Raman spectroscopy," Optics Letters **41**, 4146–4149 (2016).
12. C. C. Evans, C. Liu, and J. Suntivich, "TiO2 Nanophotonic Sensors for Efficient Integrated Evanescent Raman Spectroscopy," ACS Photonics **3**, 1662–1669 (2016).
13. T. H. Stievater, S. A. Holmstrom, D. A. Kozak, R. A. Mcgill, M. W. Pruessner, N. Tyndall, W. S. Rabinovich, and J. B. Khurgin, "Trace-Gas Raman Spectroscopy Using Functionalized Waveguides," Optica **3**, 891–6 (2016).
14. S. Schlücker, "Surface-enhanced raman spectroscopy: Concepts and chemical applications," Angewandte Chemie - International Edition **53**, 4756–4795 (2014).
15. A. Espinosa-Soria, A. Griol, and A. Martínez, "Experimental measurement of plasmonic nanostructures embedded in silicon waveguide gaps," Optics Express **24**, 9592–601 (2016).
16. F. B. Arango, A. Kwadrin, and A. F. Koenderink, "Plasmonic Antennas Hybridized with Dielectric Waveguides," ACS Nano **6**, 10156–10167 (2012).
17. F. Peyskens, A. Dhakal, P. Van Dorpe, N. Le Thomas, and R. Baets, "Surface Enhanced Raman Spectroscopy Using a Single Mode Nanophotonic-Plasmonic Platform," ACS Photonics **3**, 102–108 (2016).
18. M. Chamanzar, Z. Xia, S. Yegnanarayanan, and A. Adibi, "Hybrid integrated plasmonic-photonic waveguides for on-chip localized surface plasmon resonance (LSPR) sensing and spectroscopy." Optics Express **21**, 32086–98 (2013).
19. P. Measor, L. Seballos, D. Yin, J. Z. Zhang, E. J. Lunt, A. R. Hawkins, and H. Schmidt, "On-chip surface-enhanced Raman scattering detection using integrated liquid-core waveguides," Applied Physics Letters **90**, 1–4 (2007).
20. L. Kong, C. Lee, C. M. Earhart, B. Cordovez, and J. W. Chan, "A nanotweezer system for evanescent wave excited surface enhanced Raman spectroscopy (SERS) of single nanoparticles," Optics Express **23**, 6793 (2015).
21. S. Lin, W. Zhu, Y. Jin, and K. B. Crozier, "Surface Enhanced Raman Scattering with Ag Nanoparticles Optically Trapped by a Photonic Crystal Cavity." Nano Lett. **13**, 559–63 (2013).
22. T. R. Jensen, M. D. Malinsky, C. L. Haynes, and R. P. V. Duyne, "Nanosphere Lithography : Tunable Localized Surface Plasmon Resonance Spectra of Silver Nanoparticles," Journal of Physical Chemistry B **104**, 10549–10556 (2000).
23. M. Tabatabaei, A. Sangar, N. Kazemi-Sanjani, P. Torchio, A. Merlen, and F. Lagugné-Labarthet, "Optical Properties of Silver and Gold Tetrahedral Nanopyramid Arrays Prepared by Nanosphere Lithography," The Journal of Physical Chemistry C **117**, 14778–86 (2013).
24. M. Moskovits, "Persistent misconceptions regarding SERS," Physical Chemistry Chemical Physics **15**, 5301 (2013).
25. A. Dhakal, A. Raza, F. Peyskens, A. Z. Subramanian, S. Clemmen, N. Le Thomas, and R. Baets, "Efficiency of evanescent excitation and collection of spontaneous Raman scattering near high index contrast channel waveguides." Optics express **23**, 27391–404 (2015).
26. F. Peyskens, A. Z. Subramanian, P. Neutens, A. Dhakal, P. Van Dorpe, N. Le Thomas, and R. Baets, "Bright and dark plasmon resonances of nanoplasmonic antennas evanescently coupled with a silicon nitride waveguide," Optics Express **23**, 3088–101 (2015).
27. E. Le Ru, M. Meyer, and P. Etchegoin, "Surface Enhanced Raman Scattering Enhancement Factors: A Comprehensive Study," Journal of Physical Chemistry C **111**, 13794–13803 (2007).
28. L. Baia, M. Baia, J. Popp, and S. Astilean, "Gold films deposited over regular arrays of polystyrene nanospheres as highly effective SERS substrates from visible to NIR," Journal of Physical Chemistry B **110**, 23982–23986 (2006).
29. P. C. Wuytens, A. Z. Subramanian, W. H. De Vos, A. G. Skirtach, and R. Baets, "Gold nanodome-patterned microchips for intracellular surface-enhanced Raman spectroscopy," The Analyst **140**, 8080–8087 (2015).

1. Introduction

Silicon photonics based on high index-contrast silicon-on-insulator (SOI) waveguides has proven to be an excellent platform for biosensing. SOI enabled, amongst others, the development of sensitive and compact refractive index [1] and absorption [2] sensors across the telecom and mid-infrared wavelength range. The success of the SOI platform is largely due to the use of standard CMOS-fabrication techniques, which ensures high-volume manufacturing, reproducible components and potential CMOS compatibility. This inspired the development of a silicon nitride (SiN) counterpart, paving the way for deep-UV fabricated integrated photonics at visible wavelengths. The ongoing improvement of different optical components such as low-loss waveguides [3], spectrometers [4, 5] and hybrid integrated lasers [6] is leading to a maturation of this SiN platform [7]. Being transparent at near-infrared and visible wavelengths, SiN enables on-chip fluorescence [8] and Raman spectroscopy [9], as these scattering processes scale with λ^{-4}. Even though waveguide-based Raman spectroscopy strongly increases the collected Stokes scattering as compared to free-space sensing [10–13], it remains limited by both the low Raman cross-section of most molecules and the intrinsic background Raman scattering of the waveguide

itself [10]. Surface-enhanced Raman scattering (SERS) allows to dramatically increase the Raman signal from molecules in the close vicinity of plasmonic nano-antennas, even up to the limit of single-molecule detection [14]. Recent efforts succeeded in combining plasmonic antennas with Si [15] and SiN [16–18] waveguides, providing proof-of-concept experiments for integrated localized surface plasmon resonance (LSPR) sensing [18] and even waveguide-excited and -collected SERS [17]. However, all these approaches rely on multiple electron-beam lithography steps with critical alignment for writing both the waveguides and the nano-antennas. Apart from being time-consuming and resource-intensive, the use of e-beam lithography inhibits exploiting the full functionality of a mature integrated photonics platform. Alternative approaches combine a waveguide platform with colloidal gold or silver nanoparticles [19–21]. However, colloidal particles lack the reproducibility of top-down fabricated SERS substrates.
In this work, we develop a nanosphere-lithography [22] (NSL) based technology for patterning deep-UV fabricated SiN waveguides with gold nanotriangles. We characterize the plasmonic resonance of these nanotriangles through their absorption spectra and demonstrate efficient waveguide-based excitation and collection of surface-enhanced Raman spectra at a pump wavelength of 785 nm. Furthermore, for an equal input power we experimentally find the Stokes scattered power to be approximately equal when exciting and collecting through the waveguide versus a high numerical aperture objective. To the best of our knowledge, this is the first demonstration of an e-beam free platform for on-chip SERS, an important step towards a complete on-chip SERS-platform combining the sensing area, filters, spectrometer and even the laser on a single chip.

2. Results

Fabrication of integrated nanotriangles Fig. 1. schematically shows how a deep-UV patterned SiN chip is decorated with nanotriangles. The fabrication process is described in more detail in the methods section. First, a $2.5 - 15\,\mu m$ wide window is defined across the waveguide using photoresist. This window is thinned down using oxygen plasma to avoid stacking of the polystyrene beads. Next, polystyrene beads with a 448 nm diameter are spin-coated on the chip to form a self-assembled, hexagonally close packed monolayer in this window. These beads act as a mask for gold deposition. After lifting of the beads and resist, the waveguide is covered with a repetitive pattern of nanotriangles. Fig. 2. shows SEM images of the monolayer of beads and resulting gold nanotriangles on the waveguide. Because of the 220 nm height difference between the waveguide and the substrate, the beads form a double layer on the latter. Openings in the double HCP-layer result in the smaller nanodots visible next to the waveguide in Fig. 2(b).

Spectral properties of the localized surface plasmon resonance The nanotriangles and waveguides are designed for a Raman pump laser of 785 nm and Stokes emission at 877 nm, corresponding to the $1339\,cm^{-1}$ symmetric stretching mode (ν_s) of NO_2 in the gold-binding molecule para-nitrothiophenol (NTP) [23]. A maximal overlap of the LSPR with the wavelength region of the pump laser and Stokes emission is necessary to achieve a high SERS enhancement factor. The spectral location of this resonance strongly depends on geometrical parameters such as the size and aspect ratio of the triangles, as well as the refractive index of the surrounding materials. For uncoupled gold nanostructures, implying a large separation between the antennas, the extinction spectrum provides a reasonable indication for wavelength-dependent enhancement factor [24]. With a gap of approximately 75 nm (Fig. 2(d).), this condition is met for the nanotriangles. The optimal geometry was experimentally found by tuning the radius of the polystyrene beads, thinning down the beads with O_2 plasma (Fig. 1., between step (2) and (3)) and adjusting the thickness of the evaporated gold. Optimal values of respectively 224 nm, 15 s and 70 nm were determined from UV-Vis absorption and SERS spectra measured on different geometries using a top-down, free-space excitation (data not shown). These parameters are

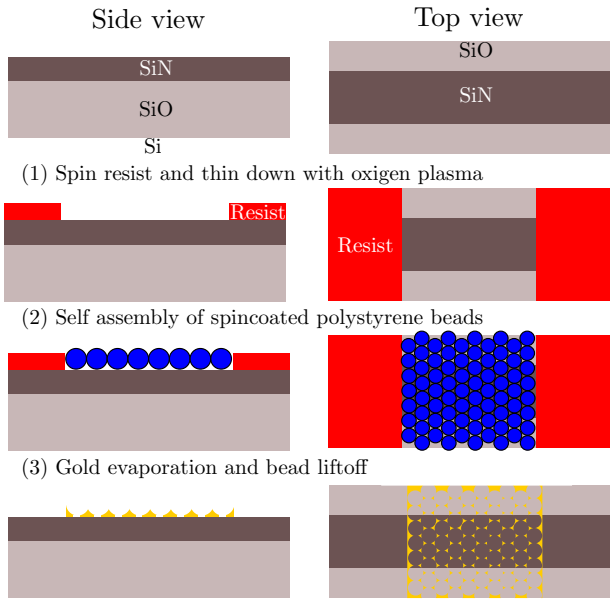

Fig. 1. Simplified processing scheme for patterning SiN waveguides with gold nanotriangles.

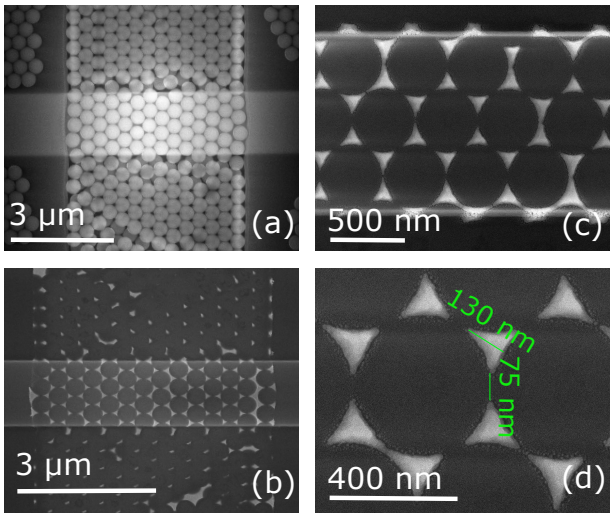

Fig. 2. SEM image of (a) a hexagonally close-packed monolayer of polystyrene beads in photoresist across the SiN waveguide and (b-d) a typical gold nanotriangle pattern on the waveguide.

used for fabricating nanotriangles on a SiN waveguide. Fig. 3(a). shows the spectral absorption from different lengths of these nanotriangle patterns on waveguides when excited by a TE polarized supercontinuum source. As expected, the absorbance increases with increasing number of nanotriangles. Furthermore, the 785 nm pump wavelength and 1339 cm^{-1} Stokes shift overlap well with this spectrum, indicating that these structures are suited for exciting surface-enhanced Raman spectra in the near-infrared. From these data we extract an absorption coefficient for the gold nanotriangles α_p of $1.7 \pm 0.5\, dB/\mu m$ at the 785 nm pump and α_s of $2.7 \pm 0.5\, dB/\mu m$ at

the 877 nm Stokes wavelength. From α_s, α_p we calculate the total collected Stokes power as function of the length of the nanotriangle section:

$$P_{col}^{R} \propto \gamma_{in}\gamma_{out} \int_0^L P_0 e^{-\alpha_p x} \sigma e^{-\alpha_s x} dx \tag{1}$$

$$\propto \gamma_{in}\gamma_{out} P_0 \sigma \frac{1 - e^{-L(\alpha_p+\alpha_s)}}{\alpha_p + \alpha_s} \tag{2}$$

Here, σ is the Raman cross-section of the molecule P_0 is the laser power incident on the entrance facet of the chip. The losses when coupling pump light in and the Stokes light out of the chip are respectively given by γ_{in} and γ_{out}. Because of the strong absorption of pump and Stokes light, after only 2.5 μm of nanotriangles the SERS signal reaches 93% of the maximum value (solid blue curve in Fig. 3(c).). Hence making the nanotriangle stretch longer does not contribute to a stronger signal. Fig. 3(c). also shows the experimentally measured intensity of the 1339 cm^{-1} SERS peak on 8 waveguides each for lengths of 2.5 μm, 5 μm, 10 μm and 15 μm, indeed showing no significant differences in signal strength with increasing length.

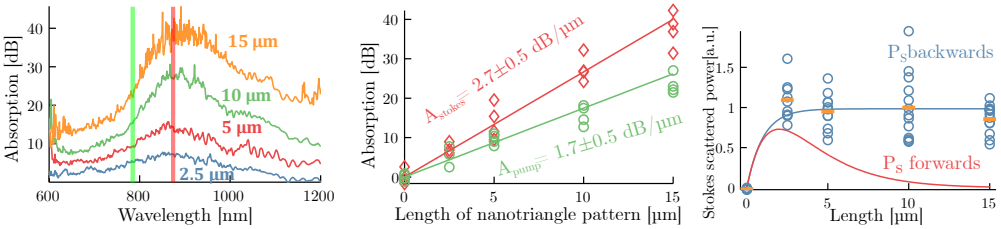

(a) (b) (c)

Fig. 3. (a) Absorption spectra of waveguides decorated with increasing lengths of nanotriangle patterns. The LSPR-absorption shows a good overlap with a 785 nm pump laser and a 1139 cm^{-1} Stokes shift, respectively green and red shaded. (b) Absorption versus nanotriangle length at pump and Stokes wavelength measured on four different waveguides for each length. A linear fit to the data gives an absorption of $2.7 \pm 0.5\ dB/\mu m$ at Stokes and $1.7 \pm 0.5\ dB/\mu m$ at the pump wavelength.(c) SERS signal strength in function of the length of the nanotriangle section, showing that the maximum signal is already reached for a 2.5 μm length. The orange bars give the average of at least 8 different measurements. The solid blue curve shows the calculated signal strength versus length when collecting the backwards Stokes scattered light in a reflection mode, as used in this work. The red curve shows the forward collected Stokes power in a transmission mode.

Surface-enhanced Raman scattering of waveguide-coupled versus free-space coupled nanotriangles SERS-spectra of the same nanotriangle patterns are measured using both free-space and waveguide-based excitation. A commercial Raman microscope is used in both cases, with the chip placed respectively perpendicular or parallel to the beam path, as shown in Fig. 4(a). This allows for an accurate comparison between the total free-space- and waveguide- collected Stokes scattered power for the same input power. Fig. 4(b). shows a camera image of the end-fire coupled chip, placed vertically under a 40x/0.6 objective installed on an upright microscope. Scattering of the waveguide-coupled pump light, propagating along the green arrow in Fig. 4.(b), can be seen at the entrance facet, at the nanotriangle section and at the other end of the waveguide. The spectra are collected in a reflection mode, meaning that the backscattered Stokes scattered light is collected by the same objective, as indicated by the dashed red arrow. The pump light propagates for approximately 1.5 mm through a multimode SiN strip waveguide

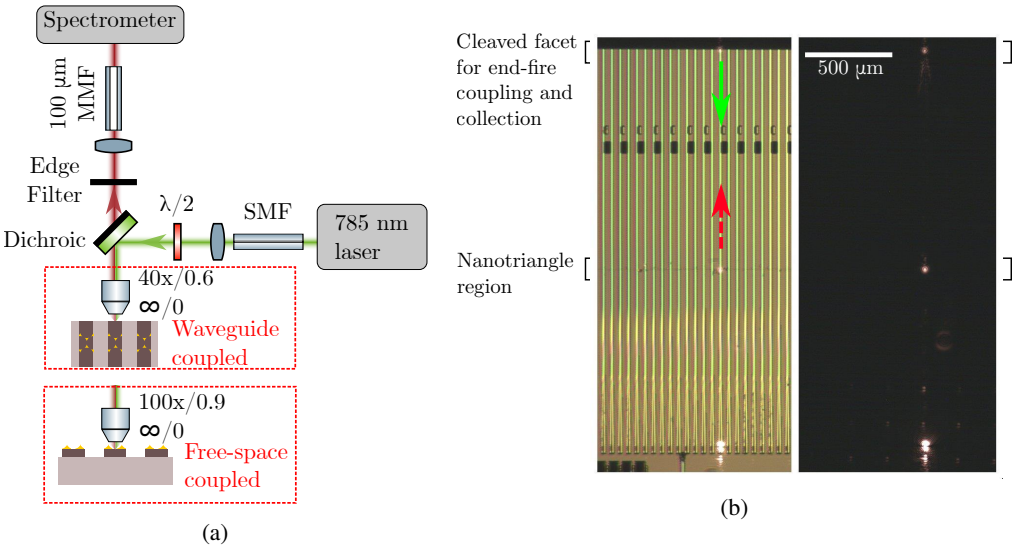

Fig. 4. (a) Schematic of the confocal microscope used for collecting Stokes scattered light from both waveguide- and free-space coupled nanotriangles. (b) Camera image of the chip in bright field (left) and dark field (right). Light is coupled from the top into the vertically oriented waveguides, and propagates along the waveguide (green arrow) until the nanotriangle section. Stokes scattered light is collected in reflection (red-dashed arrow). Scattering of the pump laser can be seen at the entrance facet and nanotriangle section.

before encountering the nanotriangle section. Along this propagation, a strong Raman signal of the SiN core is generated [10]. As a consequence, the Raman spectra collected through the waveguide consist of two major contributions, as highlighted in Fig. 5(a). One is the SERS spectrum of NTP, which in the rest of this work will be quantified by its most prominent peak at 1339 cm^{-1} ($\nu_s\, NO_2$). The other is the SiN spectrum, which for our particular SiN consists of a broad background that decreases monotonically towards longer relative frequency shifts [10] and has a characteristic peak at 2330 cm^{-1}. Note that the shape and strength of this background scales with the waveguide length and depends not only on the waveguide material but also on the exact deposition parameters. Fig. 5(a). shows a raw waveguide-excited SERS spectrum, as well as a SiN background spectrum collected from a reference waveguide without plasmonic antennas. The latter is rescaled for equal peak intensity at 2330 cm^{-1} (Fig. 5(a)., inset) because of differences in propagation length and absorption. The lack of NTP peaks on the reference spectrum also proves that the NTP peaks indeed originate from gold-bound molecules on the nanotriangles.

To compare the waveguide-excited SERS signals to a free-space excitation, we subtract the SiN background and rescale the spectrum to compensate for a total coupling loss ($\gamma_{in}\gamma_{out}$) of 8 dB. The rationale behind compensating for these coupling losses is a future integration of the spectrometer [5] and light source [6] on the chip, eliminating the need for edge-coupling and thus minimizing losses in between components. On a shorter term it is possible to substantially reduce coupling losses by optimizing the waveguide design for a specific coupling geometry. Free-space excited SERS spectra are collected top-down across the same waveguide using a 100x/0.9 NA objective, with the chip placed horizontally under the microscope. This is close to the highest possible etendue using an air objective, and thus results in the strongest possible SERS spectrum collected in free space for this particular SERS substrate. An average spectrum is calculated over the first 2.5 μm of nanotriangle pattern on the waveguide, as this part contributes to over

90% of the waveguide-coupled Raman signal. Fig. 5(b). shows both free-space and waveguide excited SERS spectra for a typical waveguide, both having the same shape and approximately equally magnitude. This comparison was made for multiple waveguides on two different chips. The integrated SERS intensity of the 1339 cm^{-1} peak for each individual nanotriangle-patterned waveguide is shown in Fig. 5(c). for both free-space and waveguide-based excitation. From this data, we conclude that exciting and collecting surface-enhanced Raman spectra through the waveguide is at least as efficient as through the high NA objective. When the guided power in the waveguide equals the power through the objective, an equal amount of Stokes scattered photons is collected by both systems. Note that this does not imply that both the field intensity and collection efficiency are individually identical in both systems. A difference in mode volume and the asymmetry of the nanotriangles on the SiN waveguide can lead to a different excitation or collection efficiency in both systems [25, 26].

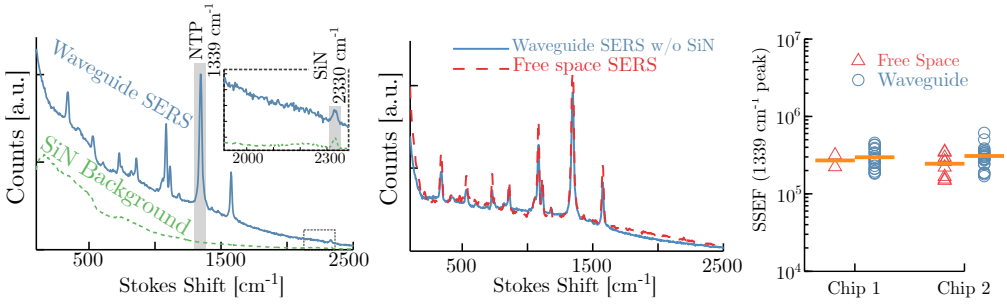

Fig. 5. (a) 4-NTP SERS signal acquired through the waveguide (solid blue) and the SiN background spectrum on a blank reference waveguide (dashed green). The 1339 cm^{-1} is used for quantifying the enhancement factor. The inset shows a characteristic peak for our SiN at 2330 cm^{-1}. (b) Waveguide collected SERS spectrum (solid blue) after subtracting the SiN background and scaling with the coupling losses, compared to a free-space collected SERS spectrum (dashed red) acquired on the same nanotriangle section. (c) SSEF for free-space excitation and collection compared to the signal strength using a waveguide-based measurement, acquired on multiple waveguides on two different chips.

To enable a quantitative comparison with other (future) integrated SERS platforms, we calculate the SERS substrate-enhancement factor for the gold nanotriangle patters as described by Le Ru et al. [27]. The SSEF is defined as the ratio between the average signal per molecule on the SERS substrate and that in a bulk, spontaneous Raman measurement:

$$SSEF = \frac{I_{SERS}}{I_{Raman}} \times \frac{N_{Vol}}{N_{Surf}} \tag{3}$$

$$= \frac{I_{SERS}}{I_{Raman}} \times \frac{H_{eff}\rho}{\mu_{Au}\mu_{NTP}A_m} = (2.5 \pm 0.7) \times 10^5 \tag{4}$$

In this definition, the intensity of the Raman and SERS signals are scaled to the same excitation power and integration time. The ratio between the number of molecules in a bulk measurement and those adsorbed on the gold surface can be calculated from the bulk molecule density ρ ($6.022 \times 10^7\ molecules/\mu m^3$), the effective height H_{eff} of the collection volume (150 μm), the density of the 4-NTP molecules on the gold μ_{NTP} ($4.4 \times 10^6\ molecules/\mu m^2$) [28], the surface area of a single nanotriangle A_m (0.023 μm^2) and the density of the metal nanostructures μ_{Au} ($11.5\ triangles/\mu m^2$). It is important to remember that, although this calculation assumes the use of exactly similar conditions (objective, microscope, pinhole etc.) for acquiring SERS and

spontaneous Raman spectra, the final enhancement factor is independent of the optical setup. An exact translation of this free-space enhancement factor to a waveguide-coupled number is not straightforward because of the intrinsic differences in both geometries, and therefore outside the scope of this paper. Qualitatively, we conclude that SERS signals are in the same order of magnitude while the number of molecules excited in both cases is similar.

3. Conclusion

In conclusion, we have demonstrated a relatively easy process for patterning individual dies of deep-UV waveguides with gold nanotriangles in a post-processing step. The absorption spectrum of this nanopattern is well suited for Raman spectroscopy in the near-infrared, a wavelength region interesting because of its low absorption by biological specimen, reasonably strong scattering and low background fluorescence. SERS data show that the SSEF of this pattern is 2.5×10^5, and that excitation and collection of SERS spectra through the waveguide is at least as efficient as using the best possible air objective. Although the enhancement factor of the nanotriangles presented in this manuscript is not among the highest reported in literature, nanosphere-lithography has also been used to fabricate high-performance SERS substrates, at least under free-space excitation [23, 28, 29]. Variations of these can possibly be combined with photonic waveguides. The hybrid integration of nano-plasmonic antennas with a mature integrated photonics platform is a prerequisite for fully integrated spectroscopic sensors. We are convinced that further technological developments on this topic will lead to breakthrough applications that are currently limited to free-space SERS sensing.

4. Methods

Fabrication As shown in Fig. 1., we start from a deep-UV patterned die containing 220 nm high by 1.4 μm wide SiN waveguides. After cleaning the chips, a $2.5 - 15$ μm wide open window is patterned in AZ MiR 701 positive photoresist using UV-contact lithography (SÜSS MA6), resulting in a resist thickness of approximately 700 nm. This resist is thinned down to less than 400 nm using O_2 plasma (Vision 320 RIE, 50 sccm O_2, 75 W, 100 mTorr, 235 s), after which the polystyrene beads are spin-coated on the chip. The resist must be thinner than the size of the polystyrene beads to avoid stacking of the beads at the edges of the window. Typically, 40 μl of a 3.75 $w\%$ in 2/1 methanol/water mixture of 448 nm polystyrene beads (Microparticles GMBH) was used for a two-step spin coating. First a HCP monolayer is formed at a speed of 2100 rpm and an acceleration of 1600 rpm/s during 45 seconds, followed by the removal of excessive beads and solvents at 5000 rpm and 1000 rpms during 40 seconds. Note that these parameters should be slightly changed depending on the chip size (4 cm^2), humidity and temperature in order to acquire an optimal arrangement of the beads into an HCP-monolayer. After spin-coating, an additional 15 s of O_2 plasma is applied. This reduces the size of the beads such that the resulting nanotriangles will have the optimal dimensions for a LSPR around 785-870 nm. The O_2 plasma also improves the adhesion of metals to the SiN surface. First a 1-4 nm Ti adhesion layer is sputtered, followed by the thermal evaporation of a 70 nm Au layer (Leybold Univex 450). Finally, the polystyrene beads are removed in dichloromethane and the resist is lifted off in acetone. The chips were characterized through scanning electron microscopy on a FEI Nova 600 Nanolab Dual-Beam FIB system, using a voltage of 18 kV and a through the lens (TLD) detection.

Transmission measurements Nanotriangle extinction spectra were measured as described by Peyskens et al. in the supplementary information of [17]. Light from an NKT EXR-4 supercontinuum source is filtered through a near-IR transmitting filter and coupled in a fiber. This fiber is plugged into a fiberbench consisting of 3 parts: an achromatic fiber collimator which converts the fiberized light to a free-space beam, a free-space broadband polarizer which

polarizes the unpolarized light into a TE-beam and an aspheric lens used to focus the free-space beam on the input facet of the chip. At the output facet a lensed fiber is used to capture the transmitted light. This lensed fiber guides the light into an optical spectrum analyzer (Advantest Q8381). Extinction spectra of the nanotriangle-covered waveguides were calculated relative to the transmission of a reference waveguide:

$$E(\lambda) = 10 \log_{10} \left[\frac{T(\lambda)^{ref}}{T(\lambda)^{NSL}} \right]$$

Chip labeling Chips were first cleaned with acetone, isopropanol and water and dried under a stream of nitrogen. Next, a short oxygen plasma (PVA-TEPLA GIGAbatch 310 M, 6000 sccm O_2, 600 W, 750 mTorr, 120 s) was used to further remove organic contaminants and render the surface hydrophilic. Immediately after, the chips were immersed for three hours in a 1 mM solution of 4-nitrothiophenol (NTP, sigma N27209) in ethanol. After incubation, the labeled chips were thoroughly rinsed with ethanol and water to remove excessive NTP molecules and again dried under a stream of nitrogen. Subsequently the chips were cleaved to allow for end-fire coupling. Three different chips were measured, in all cases the SERS spectra were acquired within 3 days after labeling.

Surface-enhanced Raman spectra All Raman spectra were acquired on a WITec Alpha 300 R+ confocal Raman microscope equipped with a 785 nm diode laser (Toptica, XTRA II) and a spectrometer using 300 lpmm grating diffracting the light onto a -70 °C cooled CCD camera (Andor iDus 401 BR-DD). Fig. 4(b). shows a sketch of the setup. All SERS spectra were measured with a laser power of 250 μW at the entrance facet of the microscope objective, and the polarization of the pump beam was set to TE using a half-wave plate. Note that a low irradiance is necessary to avoid the photoinduced reduction of p-NTP into dimercaptoazobenzene [23]. We observed this from a change in relative strength of the 1339 cm^{-1} and 1080 cm^{-1} peaks when increasing the power above 500 μW, both for waveguide- and free-space coupling. Stokes scattered light is collected in a 100 μm core multimode fiber, simultaneously functioning as confocal pinhole, for both waveguide and free-space excitation. Free-space excited spectra were acquired through a *Zeiss 100x/0.9 EC Epiplan NEOFLUAR; ∞/0* objective across the waveguide with a spatial resolution of 250 nm and an integration time of 0.23 s per pixels. Next, the average spectrum is calculated over the first 2.5 μm of nanotriangles on the waveguide, being the part of the waveguide that contributes to 95% of the signal. In the waveguide-excited case, the light was end-fire coupled into the chip using a *Nikon 40x/0.6 S Plan Fluor ELWD DIC N1; ∞/0-2.0* objective. Stokes scattered light was collected in reflection through the same objective. These spectra were acquired over 100 averages at an 0.23 s integration time.

Coupling losses The efficiency of coupling the pump laser and Stokes light respectively in- and out of the chip was quantified in a transmission measurement on the WITec Alpha 300 R microscope, where two identical objectives *Nikon 40x/0.6 S Plan Fluor ELWD DIC N1; ∞/0-2.0* are placed on both edges of the end-fire coupled chip. A total transmission loss at 785 nm of 6.2 ± 0.23 dB was measured over 6 different waveguides. We neglect propagation losses in the 2 mm long waveguides. Collecting Stokes scattering in transmission is more efficient than in reflection for waveguides with negligible loss. This is because both paths can be independently aligned for respectively the excitation wavelength of 785 nm and Stokes emission at 877 nm. In reflection, chromatic aberrations of the objective inhibit an optimal alignment. An additional loss of 1.8 ± 0.48 dB is taken into account to compensate for the difference in Raman intensity at a Stokes shift at 1339 cm^{-1} when collected in reflection as compared to transmission. This brings the total coupling loss to 8 ± 0.71 dB.

Quantification of enhancement factor SSEF The effective height of the confocal volume H_{eff} was determined from an axial scan over a TiO_2 on CaF sample, using a 200 μm multimode fiber as a pinhole:

$$H_{eff} = \int \frac{\mu_{\perp}(z)}{\mu_0} dz$$

Here, μ_0 and $\mu_{\perp}(z)$ are respectively the Raman intensity in focus and at a distance z from the focal plane. The surface area of a single nanotriangle (A_m) covered by gold-binding molecules is calculated from SEM images. The shape of the nanotriangle is approximated as a triangular-based pyramid with a 150 nm base and 75 nm height.

Funding

Research Foundation Flanders (FWO) (11U2816N, FWOKAN2014001501); Bijzonder Onderzoeksfonds Universiteit Gent (BOF) (MRP B/11267/10); European Research Council (ERC) (Inspectra 7336509).